*Desalination and Water Treatment*
www.deswater.com

doi: 10.5004/dwt.2019.24340

162 (2019) 278–289
September

# Modeling of single and binary adsorption of lead and cadmium ions onto modified olive pomace

Onur Uzunkavak[a], María Silvina Patterer[b], Franco Medici[b,*], Günseli Özdemir[a,*]

[a]*Department of Chemical Engineering, Faculty of Engineering, Ege University, 35100 Izmir, Turkey, Tel. +90 (232) 311 14 85/ +90 537 8835953; emails: gunseli.ozdemir@ege.edu.tr/gunseliozdemir3@gmail.com (G. Özdemir), onuruzunkavak@gmail.com (O. Uzunkavak)*
[b]*Department of Chemical Engineering, Materials and Environment, Faculty of Civil and Industrial Engineering, Sapienza University of Rome, Via Eudossiana 18, 00184 Rome, Italy, Tel. +39 (06) 44585568/+39 3381033667; emails: franco.medici@uniroma1.it (F. Medici), mspatterermartin@gmail.com (M.S. Patterer)*

Received 5 December 2018; Accepted 26 April 2019

**ABSTRACT**

This study deals with the evaluation of the single and binary removal of $Pb^{2+}$ and $Cd^{2+}$ from aqueous solutions using $HNO_3$ modified olive pomace (N-OP). For the specific binary adsorption behavior, a renovative isotherm model was developed based on the additivity of the single adsorption contributions of $Pb^{2+}$ and $Cd^{2+}$ calculated from the binary data. The effect of the initial metal ion concentration, pH, ionic strength, and temperature on the adsorption of the single $Pb^{2+}$ and $Cd^{2+}$, and their binary adsorption were investigated using batch experiments at the optimum conditions. The N-OP displayed maximum adsorption capacities of 64 mg $g^{-1}$ for $Pb^{2+}$ and 20.5 mg $g^{-1}$ for $Cd^{2+}$ from the single metal ion solutions using 1.0 g $L^{-1}$ N-OP. The results were best fitted with the Langmuir model for $Pb^{2+}$ and the Radke–Prausnitz model for $Cd^{2+}$ adsorption at 25°C. The reusability of the N-OP was confirmed with desorption studies. The thermodynamic study revealed that the adsorption of $Pb^{2+}$ was exothermic and that of $Cd^{2+}$ was an endothermic process. The existence of $Cd^{2+}$ in a binary solution increased the $Pb^{2+}$ removal while that of $Pb^{2+}$ reduced the $Cd^{2+}$ removal with N-OP. This behavior may contribute to a selective removal of the heavy metal ions from their mixture.

*Keywords:* Biosorption; Olive pomace; Lead; Cadmium; Binary adsorption

## 1. Introduction

The removal of heavy metals from the environment is of special importance due to their persistent nature. Conventional methods for this purpose are chemical precipitation, filtration, ion exchange, electrochemical treatment, membrane technologies, adsorption onto activated carbon, evaporation, etc. [1,2]. However, these methods are ineffective in low concentrations, and expensive because of the chemicals and energy required. Furthermore, they produce secondary toxic sludge [3]. Particular attention has recently been directed to the biosorption method which utilizes various inexpensive agro-industrial byproducts and wastes. Effectively modified biosorbents enable heavy metal reduction to very low levels and a properly developed method uses low toxic chemicals and produces low toxic waste [1,4–7].

Lead and cadmium ions are non-essential heavy metal ions for human beings, and present serious threats to the ecosystem even at low concentrations. The major industrial applications of cadmium include the production of alloys, pigments, and batteries. Lead has many different industrial,

* Corresponding authors.

agricultural, and domestic applications and is mostly used in the production of lead-acid batteries, ammunitions, paints, ceramic products, and as a solder [8].

Adsorption of heavy metal ions is controlled by the surface chemistry of the biosorbent. The binding of the heavy metal ions to the biosorbent surface with a variety of surface functional groups may occur by coordination chemistry, electrostatic interaction, and ion exchange [3,9]. Especially, oxygen containing functional groups, such as hydroxyl, carboxylic, lactonic, and phenolic, play a key role in binding heavy metal ions onto lignocellulosic biosorbents. The number of acidic surface groups can be increased by chemical treatment causing oxidation whose nature and concentration depends on the chemicals used, and the duration and temperature of the treatment [10]. The ratio of cellulose, hemicellulose, and lignin content of the lignocellulosic biomass is another factor which has an influence on the characteristics of the modified surface.

Olive pomace (OP) is an abundant agricultural waste produced in the entire Mediterranean Region, for which no important industrial use has been developed. There are studies on the sorption capacity of raw and chemically modified olive pomace and the olive stone [9–14]. OP offers prospective usage in heavy metal removal due to its sorption characteristics, excess production, large particle size for the ease of technological applications, and sludge-free operation.

The aim of this study was to obtain OP with the best sorption capacity by modification with $HNO_3$ and to test its effectiveness in the single and binary removal of $Pb^{2+}$ and $Cd^{2+}$ from aqueous solutions. For this purpose, the optimum conditions for single ion adsorption were elaborated studying the effect of the process parameters such as optimum pH, adsorbent dose, initial concentration, contact time, ionic strength, and temperature. Reusability of the biosorbent was verified with a desorption study. The binary removal of $Pb^{2+}$ and $Cd^{2+}$ was investigated using two cases: in the first case, the initial concentrations of both ions were varied concomitantly, and in the latter, initial concentration of $Pb^{2+}$ was varied in the presence of a constant background concentration of $Cd^{2+}$ since the $Cd^{2+}$ existence did not inhibit the $Pb^{2+}$ removal in the binary solutions. The modeling of adsorption kinetics for single $Pb^{2+}$ and $Cd^{2+}$, and that for the equilibrium of their single and binary solutions were further included in the study, to provide a better insight into the mechanism of the removal. To elucidate the specific binary adsorption behavior, an extended isotherm model was developed based on the addition of the single ion contributions calculated from the binary data.

## 2. Experimental

### 2.1. Materials

All the chemicals and reagents used were of analytical grade. Deionized water was used for the solution preparation. Stock solutions of 100 mg $L^{-1}$ $Pb^{2+}$, and $Cd^{2+}$ were prepared from $Pb(NO_3)_2$ (Merck, Germany), and $Cd(NO_3)_2{\cdot}4H_2O$ (Acros Organics, Belgium), respectively. Their 10, 20, 40, 60, and 80 mg $L^{-1}$ solutions were prepared using serial dilution. $HNO_3$, HCl, $NaNO_3$, and NaOH were all purchased from Merck. Raw olive pomace (R-OP) and $HNO_3$ modified olive pomace (N-OP) were used in the adsorption experiments as biosorbents.

### 2.2. Methods

#### 2.2.1. Preparation of biosorbents

The olive pomace was obtained from an olive oil plant in Pescara, Italy and was thoroughly washed with tap, and deionized water and then dried at 50°C for 24 h. It was then milled using a Groschopp & Co Mill (USA) and then sieved using Tyler standard sieves. The size fraction of 500–1,000 μm was labeled as raw olive pomace and stored in airtight containers. The OP was best modified with 2 M $HNO_3$ at 50°C for 24 h. After that, it was washed several times with deionized water, dried at 50°C for 24 h and then stored in an airtight container for further use.

#### 2.2.2. Characterization of the biosorbents

The batch equilibrium method according to Shouman et al. [15] was carried out for the determination of point of zero charge ($pH_{PZC}$). The amount of acidic and basic surface functional groups was determined using the Boehm titration method [16,17]. Freshly boiled deionized water was used for the preparation of solutions to prevent the interference of dissolved $CO_2$ and NaOH, and HCl solutions were standardized. The number of acidic sites was determined assuming that NaOH neutralizes carboxylic, lactonic, and phenolic groups, $Na_2CO_3$ neutralizes carboxylic and lactonic groups, and $NaHCO_3$ neutralizes only carboxylic groups [16]. The number of basic sites was then calculated from the amount of HCl expended in the titration [17].

The attenuated total reflection–Fourier-transform infrared spectra (ATR-FTIR) of the samples were obtained in transition mode using a PerkinElmer (Spectrum 100, Shelton, CT, USA) spectrometer in the region 4,000–400 $cm^{-1}$. The morphological features of the R-OP and N-OP were studied using a Carl Zeiss (300VP, Oberkochen, Germany) scanning electron microscope (SEM). The specific surface area of the biosorbents was calculated from the adsorption data of $N_2$ at 77 K using a BET analyzer (BET Micromeritics 3 Flex, Norcross, GA, USA). The pH adjustment of the solutions was performed with a pH meter (HI 221, Nusfalau, Romania). $Pb^{2+}$ and $Cd^{2+}$ concentrations were determined using an atomic absorption spectrometer (AAS, PerkinElmer Model, Shelton, CT, USA).

### 2.3. Adsorption study

The biosorption experiments were performed in 50 mL PP tubes using 25 mL metal ion solutions. The optimum pH values were determined by varying the pH in the range of 2 to 10 and the optimum dose of OP was determined by varying its amount in the range of 0.6–10.0 g $L^{-1}$ at the optimum pH, using 100 mg $L^{-1}$ aqueous solutions of $Pb^{2+}$ and $Cd^{2+}$, respectively. The optimum pH values were kept constant during the experiments with the addition of 0.1 M NaOH at regular intervals. In the kinetic study, the solutions with an initial $Pb^{2+}$ and $Cd^{2+}$ concentration of 100, 80, 60, 40, and 20 mg $L^{-1}$ were shaken with 1.0 g $L^{-1}$ of OP at the optimum pH as a function of time. All the experiments were performed in

duplicate. The effect of the ionic strength on the sorption process was also investigated with and without the background concentration of 0.01 and 0.1 M $NaNO_3$ with variation in the solution pH. The desorption study was investigated using 100 mg $L^{-1}$ $Pb^{2+}$ and $Cd^{2+}$ solutions adjusted to a pH of 5.5 or 6.0 and 2.5 or 3, respectively, using 0.2 M NaOH and HCl in four consecutive experiments. The thermodynamic study was accomplished at 25°C, 35°C, and 45°C using $Pb^{2+}$ and $Cd^{2+}$ solutions in the range of 10–100 mg $L^{-1}$ and the solutions were shaken with 1.0 g $L^{-1}$ of OP at the optimum pH. The adsorption experiments with binary mixtures of $Pb^{2+}$ and $Cd^{2+}$ were conducted at a 1:1 concentration ratio of these metal ions and with a background concentration of 50 and 100 mg $L^{-1}$ $Cd^{2+}$ by varying the $Pb^{2+}$ concentration in the range of 10–100 mg $L^{-1}$. Finally, the supernatant solutions were filtered and analyzed for $Pb^{2+}$ and $Cd^{2+}$ concentration using AAS.

The amount of $Pb^{2+}$ and $Cd^{2+}$ adsorbed was calculated as follows:

$$q_e = \frac{\left(C_0 - C_e\right)V}{m} \tag{1}$$

where $q_e$ is the equilibrium sorption (mg $g^{-1}$), $C_0$ and $C_e$ are the initial and equilibrium ion concentrations (mg $L^{-1}$), respectively, $V$ is the volume of solution (L), and $m$ is the amount of olive pomace (g).

### 2.4. Kinetic modeling

The kinetic results were analyzed using the kinetic models of pseudo-first-order (PFO) [18], pseudo-second-order (PSO) [19], and Weber–Morris intraparticle diffusion (IPD) [20]. The respective equations are reported below:

$$q_t = q_e\left(1 - e^{-k_1 t}\right) \tag{2}$$

$$q_t = \frac{k_2 q_e^2 t}{1 + k_2 q_e t} \tag{3}$$

$$q_t = k_{\text{ipd}} \times t^{0.5} + I \tag{4}$$

where $q_e$ and $q_t$ are the amount of $Pb^{2+}$ and $Cd^{2+}$ adsorbed at equilibrium and at time $t$ onto the OP (mg $g^{-1}$), respectively, $k_1$ is the rate constant of the PFO kinetic model ($min^{-1}$), $k_2$ is the rate constant of the PSO kinetic model (g $mg^{-1}$ $min^{-1}$), $k_{\text{ipd}}$ is the IPD model rate constant (g $mg^{-1}$ $min^{-0.5}$), and $I$ is a constant giving an idea about the effect of the boundary layer thickness (mg $g^{-1}$) [21]. When the intraparticle diffusion is the rate limiting step, $q_t$ vs. $t^{1/2}$ plot goes through the origin. However, adsorption kinetics may be controlled by film diffusion and intraparticle diffusion simultaneously. Then the straight line has an intercept.

### 2.5. Isotherm modeling

#### 2.5.1. Single ion adsorption

The three 2-parameter isotherm models of Langmuir (Eq. (5)), Freundlich (Eq. (6)), and Dubinin–Radushkevich (Eq. (7)), and the three 3-parameter isotherm models of Langmuir–Freundlich (Eq. (8)), Radke–Prausnitz (Eq. (9)), and Redlich–Peterson (Eq. (10)) were used to analyze the experimental data. Their non-linear forms are given below [21,22]:

$$q_e = \frac{q_m K_L C_e}{1 + K_L C_e} \tag{5}$$

$$q_e = K_F C^{1/n} \tag{6}$$

$$q_e = \left(q_m\right)\exp\left(-K_{D-R}\varepsilon^2\right) \tag{7}$$

$$q_e = \frac{q_m \left(K_{L-F} C_e\right)^{m_{L-F}}}{1 + \left(K_{L-F} C_e\right)^{m_{L-F}}} \tag{8}$$

$$q_e = \frac{q_m K_{R-\text{Pr}} C_e}{\left(1 + K_{R-\text{Pr}} C_e\right)^{m_{R-\text{Pr}}}} \tag{9}$$

$$q_e = \frac{K_{R-\text{Pe}} C_e}{1 + \alpha_{R-\text{Pe}}\left(C_e\right)^{\beta_{R-\text{Pe}}}} \tag{10}$$

In these expressions $q_m$ is the monolayer capacity of the adsorbent covered with metal ions (mg $g^{-1}$), $K_L$ is the Langmuir constant (L $mg^{-1}$) related to the energy of adsorption, $K_F$ is the Freundlich constant which predicts the quantity of the metal ion per gram adsorbent at the equilibrium concentration ($mg^{(1-1/n)}$ $L^{1/n}$ $g^{-1}$), and $n$ is a measure of the strength of the adsorption process and related to the surface heterogeneity. The Dubinin–Radushkevich (D-R) model has the $K_{D-R}$ as the D-R isotherm constant ($mol^2$ $kJ^{-2}$) and $\varepsilon = RT\ln\left(1 + \frac{1}{C_e}\right)$ where $R$ = 8.314 J $mol^{-1}$ $K^{-1}$ and $T$ in (K). The Langmuir–Freundlich constant $K_{L-F}$ is related to the energy of adsorption and the $m_{L-F}$ values close to zero indicates the heterogeneous sorbent, while values close to unity indicates a relatively homogeneous distribution of binding sites. The Langmuir–Freundlich isotherm coincides then with the Langmuir equation. The isotherm constants of Radke–Prausnitz ($K_{R-\text{Pr}}$), and Redlich–Peterson ($K_{R-\text{Pe}}$ and $\alpha_{R-\text{Pe}}$), and the $m_{R-\text{Pr}}$, and $\beta_{R-\text{Pe}}$ have similar meanings as explained for the Langmuir–Freundlich isotherm.

#### 2.5.2. Binary adsorption

An extended isotherm model was developed and introduced to the binary adsorption study, which is based on the addition of the single adsorption contributions of $Pb^{2+}$ and $Cd^{2+}$ calculated from the binary data. The Radke–Prausnitz and Freundlich isotherm models were applied in the modeling of the concomitant presence of $Pb^{2+}$ and $Cd^{2+}$ (Eq. (11)), whereas the Dubinin–Radushkevich and Freundlich models were performed in the modeling of the constant background concentration of the $Cd^{2+}$ system (Eq. (12)) [23,24]. The model parameters were obtained with a nonlinear statistical fit of the experimental data. The non-linear forms of the isotherm models are given below:

$$q_{\text{eq}} = \frac{q_m K_{R-\text{Pr}} C_{\text{eq,Pb}}}{\left(1 + K_{R-\text{Pr}} C_{\text{eq,Pb}}\right)^{m_{R-\text{Pr}}}} + K_F C_{\text{eq,Cd}}^{1/n} \tag{11}$$

$$q_{eq} = (q_m)\exp\left(-K_{D-R}\varepsilon^2\right) + K_F C_{eq,Cd}^{1/n} \quad (12)$$

*2.6. Thermodynamic study*

The thermodynamic study was performed using N-OP as well as with R-OP for comparison purposes. From the equilibrium data thermodynamic parameters $\Delta G°$, $\Delta H°$, and $\Delta S°$ were calculated using Eqs. (13)–(17) and the linear behavior of the $\ln K_D$ vs. $1/T$ relationship:

$$\Delta G° = -RT \ln K_D \quad (13)$$

where $\Delta G°$ is the standard free energy change, $R$ is the universal gas constant, $T$ is the temperature in Kelvin, and $K_D$ is the dimensionless distribution coefficient converted from the $K_F$ value of the Freundlich isotherm as explained by Tran et al. [25].

$$K_D = 1{,}000\ K_F \quad (14)$$

$$\ln K_D = -\frac{\Delta H°}{RT} + \frac{\Delta S°}{R} \quad (15)$$

$$-RT \ln K_D = \Delta H° - T\Delta S° \quad (16)$$

$$\Delta G° = \Delta H° - T\Delta S° \quad (17)$$

## 3. Results and discussion

*3.1. Characterization of olive pomace*

The chemical characterization provides a better understanding of the modification process of the biosorbent, and its adsorption capacity and mechanism. Goering and Van Soest analysis [26] indicated that the bulk composition of the R-OP consisted of hemicellulose (17.28%), cellulose (34.68%), lignin (31.24%), protein (7.15%), and ash (1.44%) in its dry weight. There was no starch in its content.

The point of zero charge ($pH_{PZC}$) measurements (Table 1) denoted that oxidation with $HNO_3$ made the surface of N-OP more acidic (pH 3.2) compared with the R-OP (pH 6.2). The surface functional groups obtained by Boehm's titration method (Table 1) reflected this result with the increase of the total acidity of the R-OP after the oxidation with $HNO_3$, which caused the formation of more lactonic and carboxylic groups. The effect of nitric acid used for the surface modification was ascribed to the attacks on the lignin disrupting more of the OP structure [11], and hydrolysis of some of its hemicellulose content [27]. In the oxidation process, the phenolic surface groups of lignin were decomposed and converted to carboxylic groups with a multi-step reaction process [28], which favor the adsorption of metal cations [29].

The ATR–FTIR spectra of pristine R-OP and N-OP (Fig. 1), and their loaded samples (initial $Pb^{2+}$ and $Cd^{2+}$ of 100 ppm) were evaluated to understand the nature of the surface functional groups and the possible OP-$Pb^{2+}$ and $Cd^{2+}$ interactions.

The broad band peak at 3,339 $cm^{-1}$ is due to –OH stretching vibrations which is a consequence of the inter and intra-molecular hydrogen bonding of the alcoholic, phenolic, and carboxylic groups, stemmimg from the cellulose, hemicellulose, and lignin [30,31]. The peak appeared at 2,924 $cm^{-1}$ is ascribed to the symmetric C–H stretching vibrations of the polymer backbone [11,15]. The peaks observed at 1,741 and 1,712 $cm^{-1}$ show the stretching vibration bands of C=O due to the non-ionic carboxyl groups and may be attributed to carboxylic acids or their esters. The peaks at 1,662 and 1,657 $cm^{-1}$ and 1,457 and 1,455 $cm^{-1}$ may be assigned to the asymmetric and symmetric stretching vibrations of the ionic carboxylic groups [31]. The peaks at 1,504 and 1,509 $cm^{-1}$ belong to the aromatic skeleton of lignin [32]. The bands appeared at 1,421; 1,427; 1,362; and 1,372 $cm^{-1}$ are the stretching characteristic vibrations for lignin, the bending vibration of –OH at 1,360 $cm^{-1}$ was reported for the syringyl ring of hard wood and non-wood lignins [33]. The spectra of all the lignin samples show the vibrations characteristic for the guaiacyl unit (1,260 $cm^{-1}$, G ring, and C=O stretching) [33]. Moreover, the intense band at 1,028 $cm^{-1}$ can be ascribed to the stretching vibration of the C–OH of the alcoholic groups and that of the carboxylic acids [31]. The peaks ranging from 1,000 to 1,300 $cm^{-1}$ are ascribed generally to the C–O stretching

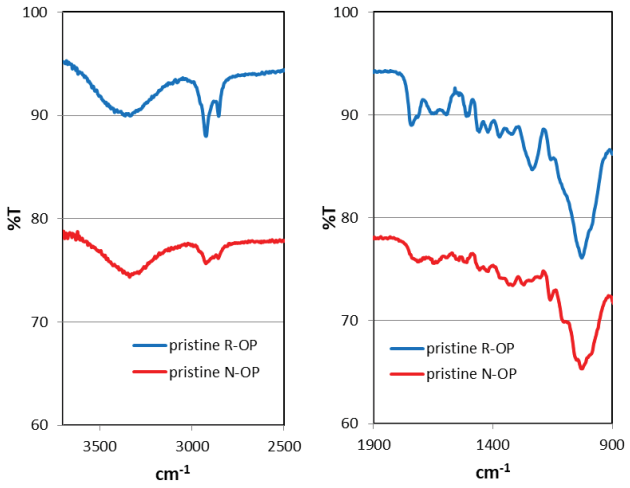


Fig. 1. ATR–FTIR spectra of R-OP and N-OP.

Table 1
Surface characteristics of the raw and $HNO_3$ modified OP

| Adsorbent type | Acidic functional groups (mmol $g^{-1}$) | | | | Basic functional groups (mmol $g^{-1}$) | $pH_{PZC}$ | Specific BET surface area ($m^2\ g^{-1}$) |
|---|---|---|---|---|---|---|---|
| | Phenolic | Lactonic | Carboxylic | Total acidity | | | |
| R-OP | 0.843 | 1.182 | 2.306 | 4.331 | 0.1084 | 6.2 | 0.1390 |
| N-OP | 0 | 1.532 | 3.145 | 4.677 | 0.1089 | 3.2 | 0.2726 |

vibration in the carboxylic acids and alcohols. The $HNO_3$ treatment increased the amount of some functional groups with single oxygen bonds such as ethers and lactones at the peak range of 1,300–1,100 $cm^{-1}$ [30]. However, this treatment also destroyed some of the bonds, which are present in R-OP. The disappearance of the peaks at 1,595 and 1,235 $cm^{-1}$ are attributed to this behavior [11].

Adsorption of $Pb^{2+}$ and $Cd^{2+}$ causes some of the peaks to shift, indicating the interference of the ions with the related surface groups due to the variation of the bond energy. The comparison of the peak locations of the R-OP indicated the shifts from 3,334 and 1,724 $cm^{-1}$ to 3,328 and 1,730 $cm^{-1}$, respectively, after $Pb^{2+}$ adsorption, and from 3,334; 2,923; 2,855; and 1,724 $cm^{-1}$ to 3,313; 2,919; 2,877; and 1,718 $cm^{-1}$ after $Cd^{2+}$ adsorption, respectively. The peak locations of the N-OP provided the shifts from 1,634 and 1,509 $cm^{-1}$ to 1,628 and 1,521 $cm^{-1}$ after $Pb^{2+}$ adsorption, and from 1,712; 1,509; 1,271; and 1,026 $cm^{-1}$ to 1,717; 1,541; 1,276; and 1,031 $cm^{-1}$ after $Cd^{2+}$ adsorption, respectively. The results pointed out that the main surface functional groups that contributed to the metal ion binding were the alcohol and carboxyl groups for both biosorbents.

Biosorbents were also characterized in terms of their surface properties using BET analysis. A large specific surface area provides high sorption capacity. The BET surface area of R-OP (0.139 $m^2 g^{-1}$) increased two times after modification (0.2726 $m^2 g^{-1}$). The improvement of the biosorption capacity was partly due to the removal of some material that caused changes in the surface area. However, the surface areas obtained describe non-porous materials.

The surface textural characterization of R-OP and N-OP was performed using SEM micrographs at various magnifications to evaluate the morphological changes on the surface. The SEM micrographs for R-OP and N-OP (Figs. 2a and b) are shown with 750× magnifications (surface was covered with gold). Fig. 2a reveals that the surface of R-OP is plain, besides some small pores are evident. Fig. 2b shows that N-OP has more pores and cavities with a rough surface structure, indicating that the acid modification removed some of the material from the surface. This explains why the BET surface area value for R-OP was lower than that of N-OP (Table 1).

### 3.2. Adsorption study

#### 3.2.1. Determination of optimum conditions for adsorption

The heavy metal amount adsorbed onto the biosorbent is strongly pH dependent. Therefore, the optimum pH of the solution for $Pb^{2+}$ and $Cd^{2+}$ adsorption using N-OP was studied with preliminary experiments. The optimum pH values were determined as 5.5 for $Pb^{2+}$ and 6.0 for $Cd^{2+}$ solutions confirmed with successive isotherm measurements (not given here).

#### 3.2.2. Effect of adsorbent dose

The effect of the adsorbent dose in the range of 0.6–10 g $L^{-1}$ on the sorption of 100 mg $L^{-1}$ $Pb^{2+}$ and $Cd^{2+}$ from a solution was investigated at the optimum pH values. The data revealed that the adsorbent dose significantly influenced the extent of $Pb^{2+}$ and $Cd^{2+}$ adsorbed (Fig. 3). At low R-OP and N-OP dose, the adsorption capacities for $Pb^{2+}$ and $Cd^{2+}$ were 30 and 82.5 mg $g^{-1}$ for $Pb^{2+}$, and 5 and 18 mg $g^{-1}$ for $Cd^{2+}$, respectively. However, a higher adsorbent dose resulted in a lower adsorption capacity. This result confirms that at a low adsorbent dose, all types of sites are exposed to adsorption, whereas at a high adsorbent dose, only the adsorption sites of higher energy are available [34]. Therefore, the optimum adsorbent dose for R-OP and N-OP was selected as 1.0 g $L^{-1}$ and used throughout the study.

#### 3.2.3. Kinetic study and modeling

The contact time was also evaluated as an important factor affecting the sorption efficiency. The sorption capacity of N-OP at varying initial $Pb^{2+}$ and $Cd^{2+}$ concentrations was studied as a function of time (Fig. 4). While the adsorption equilibrium was achieved at low $Pb^{2+}$ and $Cd^{2+}$ concentrations within 3–4 h, at higher concentrations equilibrium was reached within 10–15 h. Hence, equilibrium time was found to be dependent on the initial ion concentration.

The pseudo-first-order and pseudo-second-order kinetic models originate from chemical reaction kinetics and the adsorption rate is based on the adsorption capacity [35]. Modeling of the kinetic studies indicated that the

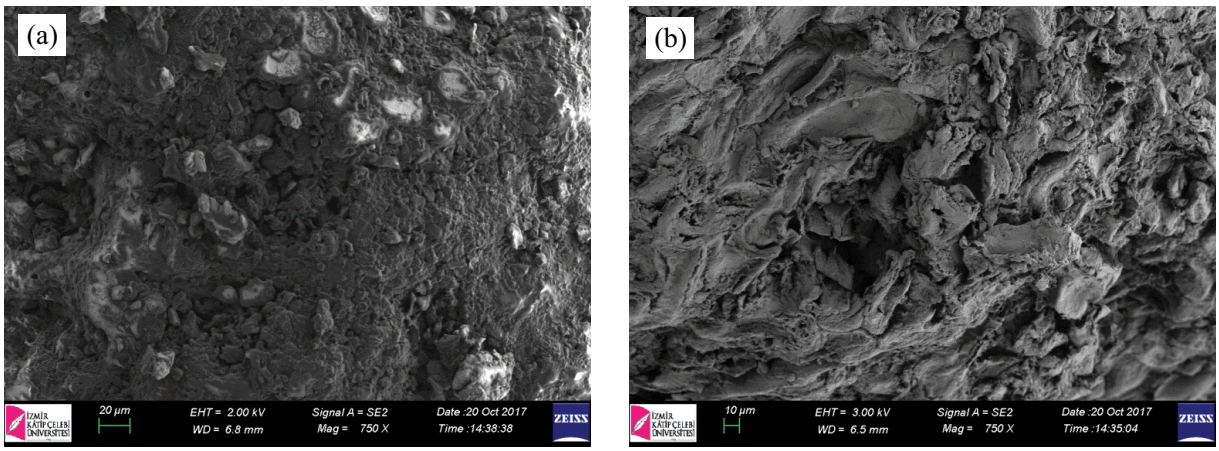


Fig. 2. SEM images of (a) R-OP and (b) N-OP.

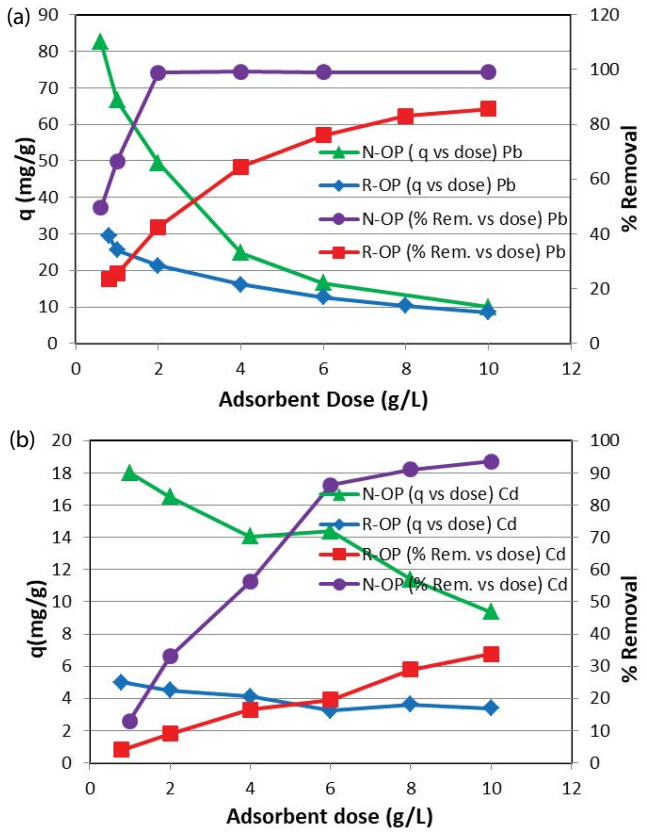


Fig. 3. Effect of the R-OP and N-OP dose on the adsorption capacity and removal extent of (a) $Pb^{2+}$ and (b) $Cd^{2+}$.

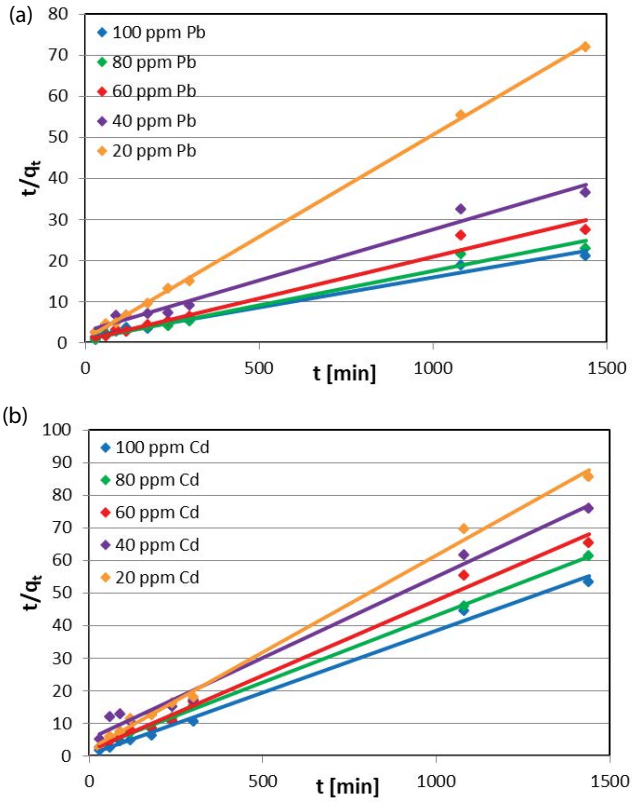


Fig. 4. Effect of contact time, and initial concentration on (a) $Pb^{2+}$ and (b) $Cd^{2+}$ adsorption onto N-OP (linear presentation with pseudo-second-order model).

adsorption of $Pb^{2+}$ and $Cd^{2+}$ followed a pseudo-second-order equation. The chemical reaction models are based on the whole process of adsorption. On the other hand, the adsorption diffusion models are derived from three consecutive steps: (1) diffusion across the liquid film surrounding the adsorbent particles, referred to external diffusion or film diffusion, (2) diffusion in the liquid contained in the pores and/or along the pore walls, referred to internal diffusion or intraparticle diffusion, and (3) adsorption between the adsorbate and active sites. Consequently, adsorption diffusion models can represent the real adsorption course more reasonably, and are useful for the design of fixed-bed systems [35]. To evaluate the diffusion mechanism of the present study, the parameters of the Weber–Morris intraparticle diffusion model were determined. Two linear sections resulting from the model revealed that the external diffusion was the controlling step in the adsorption process (Table 2).

### 3.2.4. Equilibrium study and modeling

The adsorption capacity of N-OP was 64 mg $g^{-1}$ for $Pb^{2+}$ and 20.5 mg $g^{-1}$ for $Cd^{2+}$, and that of R-OP was 33 mg $g^{-1}$ for $Pb^{2+}$ and 8 mg $g^{-1}$ for $Cd^{2+}$. The steep isotherm feature (Fig. 5) obtained with N-OP revealed that N-OP beneficially adsorbs at low $Pb^{2+}$ and $Cd^{2+}$ concentrations when compared with R-OP. This behavior is caused by the formation of acidic adsorption sites with a high energy level that leads to strong adsorption at low equilibrium concentrations [36]. The presence of a higher amount of acidic groups, mainly carboxylic, ionized on the N-OP at a pH of 5.5–6.0 justifies this behavior (Table 1). The decrease in the solution pH during the $Pb^{2+}$ and $Cd^{2+}$ adsorption onto the N-OP further showed that the mechanism of the process was mainly an ion exchange between the ionizable protons of the surface oxygen groups and divalent cations. The R-OP ($pH_{PZC}$ = 6.2) adsorbed a considerable amount of $Pb^{2+}$ and $Cd^{2+}$, however, this adsorption may not be ascribed to the proton exchange mechanism. Then, the pH of the solution remained constant during adsorption of $Pb^{2+}$ and $Cd^{2+}$ onto the R-OP. Nonetheless, the shift of the carboxylic peaks in contact with the $Pb^{2+}$ and/or $Cd^{2+}$ detected in the ATR–FTIR spectra may occur with the exchange with other ions such as $Na^{+}$ or $Ca^{2+}$.

The equilibrium data obtained at 298 K with R-OP and N-OP using $Pb^{2+}$ and $Cd^{2+}$ were correlated fitting the three 2-parameter and three 3-parameter isotherm models. The Langmuir, Freundlich, and Dubinin–Radushkevich models were the 2-parameter models calculated and the Langmuir–Freundlich, Radke–Prausnitz, and Redlich–Peterson isotherms were the 3-parameter models studied with the corresponding deviation percentage ($\Delta Q\%$) and the root mean square error (RMSE) using the solver add-in function (Microsoft Excel). The values of the isotherm parameters showed that the Langmuir isotherm for the $Pb^{2+}$ adsorption, and the Radke–Prausnitz isotherm for $Cd^{2+}$ adsorption were the best simulating models for N-OP (Table 3). However, the

Table 2
Kinetic model parameters for $Pb^{2+}$ and $Cd^{2+}$ adsorption onto N-OP

| Heavy metal ion | $C_0$ (mg $L^{-1}$) | $q_{exp}$ (mg $g^{-1}$) | Pseudo-first-order | | | | Pseudo-second-order | | | | Intraparticle diffusion | | | |
|---|---|---|---|---|---|---|---|---|---|---|---|---|---|---|
| | | | $q_{calc}$ (mg $g^{-1}$) | $k_1$ (L $min^{-1}$) | $R^2$ | RMSE | $q_{calc}$ (mg $g^{-1}$) | $k_2$ (g $mg^{-1}$ $min^{-1}$) | $R^2$ | RMSE | $k_{ipd}$ (mg $g^{-1}$ $h^{-0.5}$) | $I$ (mg $g^{-1}$) | $R^2$ | RMSE |
| $Pb^{2+}$ | 100 | 68 | 67.6083 | 0.0016 | 0.7423 | 15.2798 | 67.5676 | 0.0002 | 0.9876 | 6.5933 | 5.5654 | 37.7930 | 0.8276 | 7.4894 |
| | 80 | 63 | 61.6595 | 0.0016 | 0.5376 | 19.3245 | 60.2410 | 0.0003 | 0.9771 | 8.8002 | 16.4785 | 19.5483 | 0.5881 | 19.1179 |
| | 60 | 52.5 | 52.4807 | 0.0016 | 0.4298 | 17.5631 | 49.2611 | 0.0006 | 0.9766 | 5.1421 | 13.9690 | 18.1888 | 0.6797 | 17.1415 |
| | 40 | 39.5 | 38.9045 | 0.0015 | 0.7857 | 6.2626 | 40.3226 | 0.0002 | 0.9837 | 3.3289 | 14.794 | −2.1412 | 0.7520 | 14.1514 |
| | 20 | 20 | 19.9526 | 0.0019 | 0.2031 | 7.6182 | 20.1207 | 0.0029 | 0.9995 | 1.1959 | 4.8721 | 9.7498 | 0.7063 | 5.9861 |
| $Cd^{2+}$ | 100 | 27 | 26.3027 | 0.0018 | 0.4417 | 11.2325 | 26.2467 | 0.0031 | 0.9944 | 2.1769 | 5.3889 | 15.5740 | 0.6020 | 7.1610 |
| | 80 | 23.5 | 23.4423 | 0.0020 | 0.7243 | 6.1063 | 24.3309 | 0.0009 | 0.9990 | 1.4016 | 1.6174 | 16.0326 | 0.9440 | 2.8333 |
| | 60 | 22 | 21.8776 | 0.0017 | 0.0765 | 7.0655 | 21.6450 | 0.0013 | 0.9932 | 1.8582 | 8.6905 | 4.4661 | 0.9194 | 11.2848 |
| | 40 | 19 | 19.0546 | 0.0016 | 0.6244 | 3.5294 | 19.9601 | 0.0005 | 0.9902 | 1.7288 | 8.8783 | −2.0817 | 0.9256 | 9.6658 |
| | 20 | 16.8 | 16.9824 | 0.0018 | 0.1839 | 5.3463 | 16.7785 | 0.0017 | 0.9964 | 1.6493 | 3.9698 | 6.9793 | 0.7500 | 4.3640 |

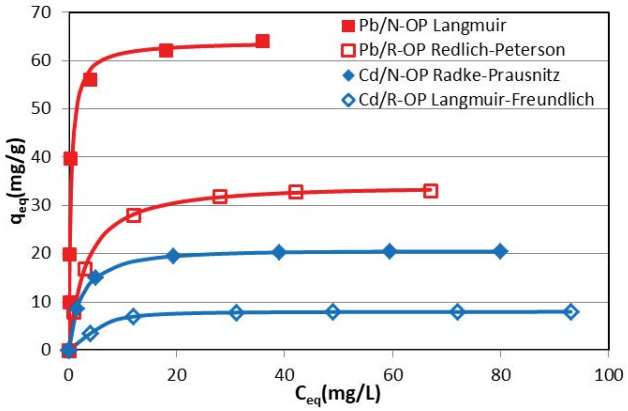


Fig. 5. Equilibrium study as a function of the initial $Pb^{2+}$ and $Cd^{2+}$ concentration onto R-OP and N-OP at 25°C.

Redlich–Peterson and Langmuir–Freundlich isotherms fitted the best for $Pb^{2+}$ and $Cd^{2+}$ adsorption onto R-OP, respectively (Fig. 5). The Langmuir–Freundlich model becomes the Freundlich isotherm at low ion concentrations, and converts to the Langmuir isotherm at higher concentrations. The Radke–Prausnitz and Redlich–Peterson isotherm models are also a combination of elements from both the Langmuir and Freundlich equations. At high ion concentrations the Redlich–Peterson and Radke–Prausnitz models reduce to the Freundlich isotherm, and when $\beta = 1$ for the Redlich–Peterson model and $m_{R-Pr} = 0$ for the Radke–Prausnitz model they become the Langmuir isotherm [37]. The Radke–Prausnitz model gives a good fit over a wide range of ion concentration.

### 3.2.5. Effect of pH and ionic strength

The pH of the solution affects not only the speciation behavior of heavy metal ions but also the protonation of the functional groups on the biosorbent. The effect of the solution pH on the $Pb^{2+}$ and $Cd^{2+}$ adsorption using N-OP was studied over the range of 2–12 to obtain the optimum pH. The results exhibited a strong pH dependence for biosorption (Fig. 6). A sharp increase in the sorption capacity above 5.5 for $Pb^{2+}$ and 6 for $Cd^{2+}$ until reaching a pH of 8, indicates that in addition to the adsorption of $Pb^{2+}$ and $Cd^{2+}$, $Pb(OH)^+$, and $Cd(OH)^+$ are formed and captured by the biosorbent, restricting the true biosorption process. Consequently, the optimum pH values for adsorption were chosen as 5.5 and 6.0 for the $Pb^{2+}$ and $Cd^{2+}$ solutions, respectively. However, at pH values higher than 8, a decrease in the biosorption capacity may be attributed to the formation of solid $Pb(OH)_2$, and $Cd(OH)_2$ by precipitation, and their anionic hydroxide complexes which decrease their interaction with the negatively charged active sites. The figures further show that at low pH values, $H^+$ compete with $Pb^{2+}$ and $Cd^{2+}$ so that no adsorption occurs at a pH value of 2.0 and lower for $Pb^{2+}$, and 3.0 and lower for $Cd^{2+}$ solutions. As the pH increases above these values, ($pH_{PZC} = 3.2$ for N-OP) the surface functional groups become more and more negatively charged with subsequent attraction of $Pb^{2+}$ and $Cd^{2+}$, indicating that interactions are electrostatic in nature and an ion exchange mechanism may take place [4,29,38].

Table 3
Isotherm model parameters for the adsorption of $Pb^{2+}$ and $Cd^{2+}$ onto R-OP and N-OP

| Heavy metal ion | Adsorbent | Isotherm model | $q_m$ | $K$ | $m$ | $\alpha$ | $\beta$ | $\Delta Q\%$ | RMSE |
|---|---|---|---|---|---|---|---|---|---|
| $Pb^{2+}$ | N-OP | Langmuir | 64 | 2.28 | | | | 0.68 | 6.58 |
| | R-OP | Redlich–Peterson | | 10.69 | | 0.28 | 1.02 | 0.46 | 0.24 |
| $Cd^{2+}$ | N-OP | Radke–Prausnitz | 20.5 | 0.38 | 1.03 | | | 0.01 | 0.03 |
| | R-OP | Langmuir–Freundlich | 8 | 0.22 | 2 | | | 0.17 | 0.03 |

As wastewaters usually contain electrolytes in high concentrations, the adsorption behavior was also considered with the addition of salts. The metal uptake is sensitive to changes in electrolyte concentration if the ion exchange and electrostatic attraction are the ruling mechanisms for metal ion removal [39]. Therefore, the effect of the ionic strength (0.01 and 0.1 M $NaNO_3$) as a function of pH on the adsorption of $Pb^{2+}$ and $Cd^{2+}$ onto N-OP were also studied and interpreted in terms of their adsorption mechanisms (Fig. 6). The results showed that the increase in ionic strength from 0.01 to 0.1 M had a moderate effect on the adsorption of $Pb^{2+}$ and $Cd^{2+}$ until reaching a pH of 5.5 to 6.0, indicating that the ion exchange and electrostatic attraction play a role in the removal of $Pb^{2+}$ and $Cd^{2+}$ with N-OP. At pH values higher than 3–4, carboxyl groups of the lignocellulosic materials ($pH_{PZC}$ = 3.2 for N-OP) are gradually deprotonated and negatively charged, as considered in the pH effect [39].

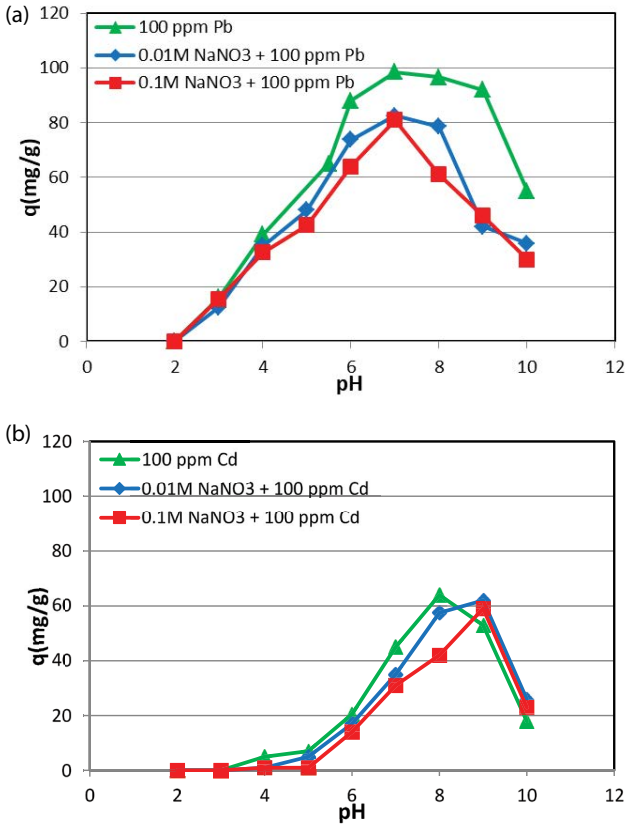


Fig. 6. Effect of pH and ionic strength of 0.01 and 0.1 M $NaNO_3$ on the adsorption capacity of N-OP for (a) $Pb^{2+}$ and (b) $Cd^{2+}$ removal.

*3.2.6. Thermodynamic study*

An increase or decrease in temperature causes a change in the amount of heavy metal adsorbed by the biosorbent. The results showed that (Fig. 7) the sorption capacity of N-OP for $Pb^{2+}$ decreased and that for $Cd^{2+}$ increased with an increase in the temperature indicating that the adsorption of $Pb^{2+}$ was exothermic and that of $Cd^{2+}$ was an endothermic process. On the other hand, the R-OP exhibited an endothermic sorption behavior for both $Pb^{2+}$ and $Cd^{2+}$ (Table 4 and Fig. 7). The thermodynamic parameters provide valuable information about the sorption mechanism. The negative values of $\Delta G°$ calculated state that all the processes are feasible and spontaneous. A negative value of $\Delta H°$ specifies an exothermic, and a positive value an endothermic process. The negative value of $\Delta H°$ for $Pb^{2+}$ adsorption onto N-OP

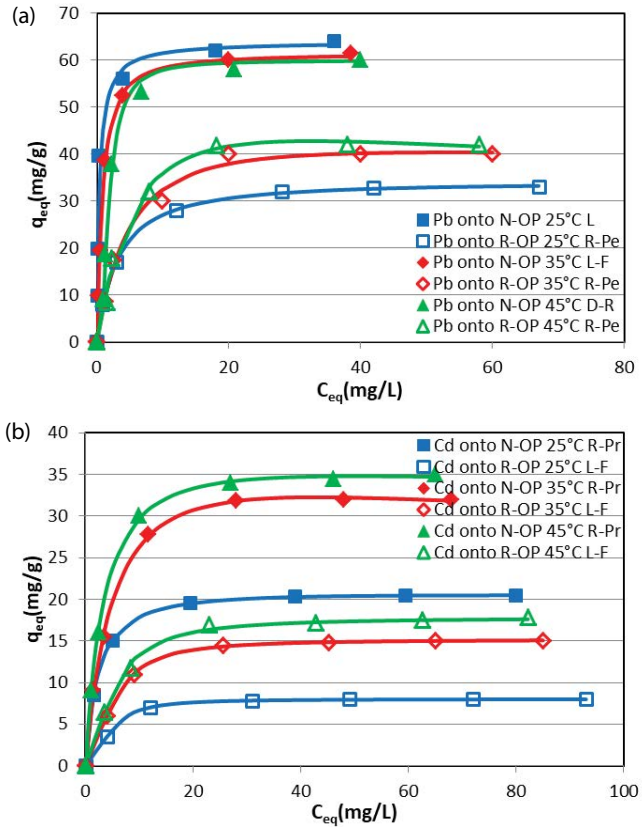


Fig. 7. Equilibrium study as a function of initial (a) $Pb^{2+}$ and (b) $Cd^{2+}$ concentration onto R-OP and N-OP at different temperatures.

Table 4
Thermodynamic parameters calculated for $Pb^{2+}$ and $Cd^{2+}$ adsorption onto R-OP and N-OP at different temperatures

| Metal ion | Adsorbent | $T$ (K) | $\ln K_D$ | $\Delta G°$ (kJ mol$^{-1}$) | $\Delta H°$ (kJ mol$^{-1}$) | $\Delta S°$ (J mol$^{-1}$ K$^{-1}$) |
|---|---|---|---|---|---|---|
| $Pb^{2+}$ | R-OP | 298 | 9.46 | –23.446 | 6.018 | 98.896 |
| | | 308 | 9.55 | –24.457 | | |
| | | 318 | 9.62 | –25.423 | | |
| | N-OP | 298 | 10.47 | –25.951 | –16.552 | 31.672 |
| | | 308 | 10.31 | –26.390 | | |
| | | 318 | 10.05 | –26.579 | | |
| $Cd^{2+}$ | R-OP | 298 | 8.22 | –20.370 | 23.253 | 146.913 |
| | | 308 | 8.72 | –22.329 | | |
| | | 318 | 8.81 | –23.287 | | |
| | N-OP | 298 | 9.24 | –22.902 | 11.379 | 115.089 |
| | | 308 | 9.41 | –24.103 | | |
| | | 318 | 9.53 | –25.201 | | |

asserts that $Pb^{2+}$ adsorption is strong and controlled by the enthalpic effect, favoring its adsorption at low temperatures. On the other hand, the positive value of $\Delta H°$ for $Cd^{2+}$ adsorption is due to the entropic effect and favors the higher temperatures for $Cd^{2+}$ adsorption (Fig. 7). The high positive values of $\Delta S°$ (Table 4) pointed out an increased disorder at the solid–solution interface, supporting additionally the ion exchange mechanism. The different thermodynamic features of $Pb^{2+}$ and $Cd^{2+}$ adsorption onto N-OP may contribute to a selective removal of the heavy metal ions from the binary solution.

The modeling of the isotherms at different temperatures showed that $Pb^{2+}$ adsorption onto N-OP conformed to the Langmuir isotherm at 25°C, while at higher temperatures the Langmuir–Freundlich and Dubinin–Radushkevich models fitted better (Fig. 7a). For $Pb^{2+}$ adsorption onto R-OP the best fit was with the Redlich–Peterson model at three different temperatures. Similarly, the adsorption of $Cd^{2+}$ onto N-OP and R-OP resulted in the same sorption isotherms of Radke–Prausnitz and Langmuir–Freundlich at three different temperatures, respectively (Fig. 7b).

### 3.2.7. Desorption study

The feasible reuse of N-OP was investigated with a desorption study. The study was carried out using a batch process first adjusting the solution pH to 5.5 and 6.0 with NaOH for 100 mg L$^{-1}$ $Pb^{2+}$ and $Cd^{2+}$ solutions, for the adsorption, and then to a pH 2 and 3 with $HNO_3$ for the desorption, respectively, with four repetitions of the adsorption–desorption cycle. A high level of desorption (Fig. 8) attained with $Pb^{2+}$ and $Cd^{2+}$ was attributed to the mechanism of the ion exchange which is reversible [40]. Consequently, the regenerative and reusable properties of N-OP make it a suitable biosorbent for practical use.

### 3.2.8. Binary adsorption

The sorption capacity of a biosorbent of one metal ion in a binary metal ion solution compared with that of its single ion system may be higher, lower or the same depending on the synergistic/antagonistic effect or no interaction [32]. The adsorption behavior of N-OP in single and binary ion systems of $Pb^{2+}$ and $Cd^{2+}$ was investigated. Two types of binary adsorption studies were carried out such as $Pb^{2+}$ and $Cd^{2+}$ adsorption at a 1:1 $Pb^{2+}$ to $Cd^{2+}$ ratio in the range of 10–100 mg L$^{-1}$ initial concentrations, and adsorption of $Pb^{2+}$ with varying initial concentration of 10–100 mg L$^{-1}$ at the

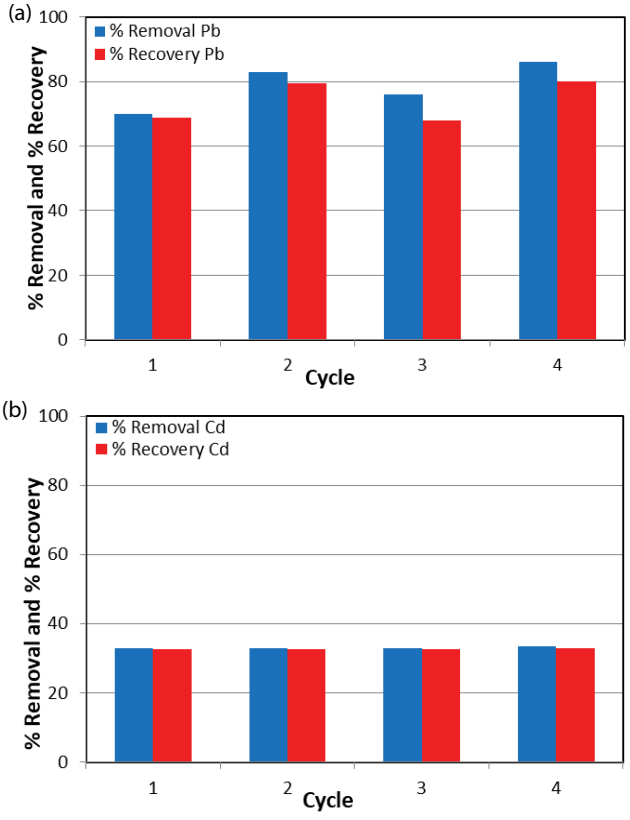


Fig. 8. Adsorption and desorption behavior of (a) $Pb^{2+}$ and (b) $Cd^{2+}$ ($C_{in}$: 100 mg L$^{-1}$) onto and from N-OP as a function of % removal and % recovery in four cycles.

Table 5
Parameters of the binary adsorption isotherm models

| Binary system | Ion | Isotherm model | $q_m$ | $K_F$ | $K$ | $n$ | $m$ | ΔQ% | RMSE |
|---|---|---|---|---|---|---|---|---|---|
| 1:1 | $Pb^{2+}$ | Radke-Prausnitz and Freundlich | 64 | 5.54 | $3.6 \times 10^{-4}$ | 1.86 | 2.35 | 0.03 | 0.85 |
| | $Cd^{2+}$ | | 11 | 5.53 | 26.59 | 7.59 | 1.76 | 0.45 | 0.53 |
| 50 ppm $Cd^{2+}$ | $Pb^{2+}$ | Dubinin–Radushkevich and Freundlich | 77 | $5.8 \times 10^{-6}$ | $2.3 \times 10^{-4}$ | 0.24 | | 9.47 | 3.87 |
| 100 ppm $Cd^{2+}$ | | | 64 | $3.0 \times 10^{-7}$ | $1.9 \times 10^{-4}$ | 0.25 | | 8.98 | 7.95 |

constant background concentrations of 50 and 100 mg $L^{-1}$ $Cd^{2+}$, respectively. The results showed that when the initial concentrations of both $Pb^{2+}$ and $Cd^{2+}$ were varied at a 1:1 ratio in the binary system, $Cd^{2+}$ did not hinder the adsorption of $Pb^{2+}$ in the range of 0–20 mg $L^{-1}$, however, at higher initial concentrations (Fig. 9a) the sorption of $Pb^{2+}$ was first suppressed and then increased again until having the same capacity at 100 mg $L^{-1}$ $Pb^{2+}$ with that of the single $Pb^{2+}$ adsorption. The figure further shows that the adsorption capacity of $Cd^{2+}$ in the presence of $Pb^{2+}$ decreased to half of its single ion sorption capacity. A similar behavior of $Pb^{2+}$ adsorption at the constant background $Cd^{2+}$ concentration of 50 and 100 mg $L^{-1}$ was observed (Fig. 9b), pointing out that the adsorbed $Pb^{2+}$ amount remained lower between 20 and 80 mg $L^{-1}$ of its initial concentration compared with its single ion adsorption and then increased, reaching values above its single ion concentrations indicating a synergistic effect at high $Pb^{2+}$ concentrations. This outcome indicates that at low and high $Pb^{2+}$ and $Cd^{2+}$ concentrations, $Pb^{2+}$ adsorption was preferential. The preferential adsorption changing with the ion concentration in the medium was ascribed to the existence of two or more types of sites on N-OP [41]. The FTIR results of the loaded R-OP and N-OP revealed the related sites which were common for both ions and specific for $Pb^{2+}$ or $Cd^{2+}$, respectively.

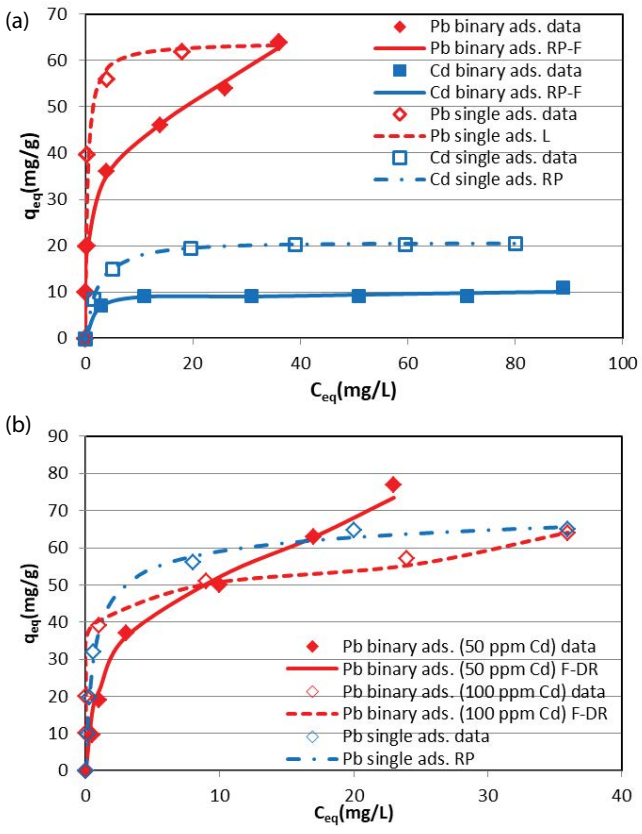


Fig. 9. Comparison of single and binary $Pb^{2+}$ adsorption in a mixture with $Cd^{2+}$ onto N-OP, (a) 1:1 ratio in the binary system and (b) variation of $Pb^{2+}$ concentration at 50 and 100 ppm $Cd^{2+}$ background concentration.

The modified and extended Langmuir and Freundlich models given in the literature [24,41] were not able to describe the adsorption behavior of the N-OP from the binary $Pb^{2+}$ and $Cd^{2+}$ solutions. For the modeling of the specific behavior of the binary adsorption, an extended model was developed in which the addition of the single isotherm contributions was calculated with the binary data (Table 5). The $Pb^{2+}$ adsorption conformed to the Radke–Prausnitz and that of $Cd^{2+}$ to the Freundlich models in the 1:1 ion solutions and $Pb^{2+}$ adsorption to the Dubinin–Radushkevich and that of $Cd^{2+}$ again to the Freundlich models in the constant background concentration of $Cd^{2+}$. The models pointed out the single sorption behavior of ions from the binary mixture as an additive contribution [23,41]. The affinity in the adsorption capacities of the biosorbent toward $Pb^{2+}$ were ascribed to both a larger ionic radius and the electronegativity than those of $Cd^{2+}$ as $Pb^{2+}$ (1.19 Å; 2.33) > $Cd^{2+}$ (0.97 Å; 1.69) [29,42]. However, the sorption capacity may change depending on the lignocellulosic source and the nature of the related surface functional groups [39].

## 4. Conclusions

This study indicates that $HNO_3$ modified olive pomace is a promising biosorbent having a sorption capacity for $Pb^{2+}$ three times higher than that for $Cd^{2+}$. The point of zero charge measurements revealed that the surface charge of the N-OP becomes negative above pH 3.2 which accounts for the enhanced sorption at the optimum pH values of 5.5 and 6.0 for $Pb^{2+}$ and $Cd^{2+}$, respectively, with a sorption mechanism of ion exchange and electrostatic interaction. The adsorption kinetics was best explained with a pseudo-second-order kinetic model. Except for the $Pb^{2+}$ adsorption onto N-OP which is best predicted with the Langmuir isotherm model, the three parameter models provided a better fit for the equilibrium data, reflecting the inhomogeneous nature of the surface. Adsorption of $Pb^{2+}$ was favored in the presence of $Cd^{2+}$ in the binary system, while $Cd^{2+}$ adsorption

was reduced. Isotherm models were developed for the first time by the researchers of this study based on the additive behavior of the single adsorption contributions of $Pb^{2+}$ and $Cd^{2+}$ calculated from binary data which was able to explain the specific behavior of the binary equilibrium. The N-OP could be successfully regenerated using desorption experiments. The $Pb^{2+}$ uptake is spontaneous and exothermic and that of $Cd^{2+}$ is spontaneous and endothermic in nature. This opposite behavior may be used in the selective removal of $Pb^{2+}$ from mixtures with $Cd^{2+}$.

## Acknowledgment

The authors are thankful to Ege University Research Fund for the financial support under Project No 14-MUH-052.

## References

[1] J. Wang, C. Chen, Biosorbents for heavy metals removal and their future, Biotechnol. Adv., 27 (2009) 195–226.
[2] M.A. Barakat, New trends in removing heavy metals from industrial wastewater, Arabian J. Chem., 4 (2011) 361–377.
[3] A. Abdolali, H.H. Ngo, W. Guo, J.L. Zhou, B. Du, Q. Wei, X.C. Wang, P.D. Nguyen, Characterization of a multi-metal binding biosorbent: chemical modification and desorption studies, Bioresour. Technol., 193 (2015) 477–487.
[4] I.-H. Liao, J.-H. Huang, S.-L. Wang, M.-P. Cheng, J.-C. Liu, Adsorptions of Cd(II) and Pb(II) in aqueous solution by rice-straw char, Desal. Wat. Treat., 57 (2016) 21619–21626.
[5] C.K. Jain, D.S. Malik, A.K. Yadav, Applicability of plant based biosorbents in the removal of heavy metals: a review, Environ. Process., 3 (2016) 495–523.
[6] V. Javanbakht, S.A. Alavi, H. Zilouei, Mechanisms of heavy metal removal using microorganisms as biosorbent, Water Sci. Technol., 69 (2014) 1775–1787.
[7] Y. Qie, J. Wang, W. Zhou, B. Gao, Y. Zhang, Evaluation of a deep-sea mesophilic bacteria exopolysaccharides in removal of low concentration Pb(II) from aqueous medium, Desal. Wat. Treat., 28 (2011) 174–182.
[8] P.B. Tchounwou, C.G. Yedjou, A.K. Patlolla, D.J. Sutton, Heavy metal toxicity and the environment, Mol. Clin. Environ. Toxicol., 101 (2012) 133–164.
[9] F. Pagnanelli, S. Mainelli, F. Veglio, L. Toro, Heavy metal removal by olive pomace: biosorbent characterisation and equilibrium modelling, Chem. Eng. Sci., 58 (2003) 4709–4717.
[10] M.A. Martin-Lara, F. Pagnanelli, S. Mainelli, M. Calero, L. Toro, Chemical treatment of olive pomace: effect on acid-basic properties and metal biosorption capacity, J. Hazard. Mater., 156 (2008) 448–457.
[11] M.A. Martin-Lara, G. Blazquez, A. Ronda, A. Pérez, M. Calero, Development and characterization of biosorbents to remove heavy metals from aqueous solutions by chemical treatment of olive stone, Ind. Eng. Chem. Res., 52 (2013) 10809–10819.
[12] A.L. Fernando, S. Monteiro, F. Pinto, B.S. Mendes, Production of biosorbents from waste olive cake and its adsorption characteristics for $Zn^{2+}$ ion, Sustainability, 1 (2009) 277–297.
[13] A. Aziz, M.S. Ouali, E.H. Elandaloussi, L.Ch. De Menorval, M. Lindheimer, Chemically modified olive stone: a low-cost sorbent for heavy metals and basic dyes removal from aqueous solutions, J. Hazard. Mater., 163 (2009) 441–447.
[14] A. Ronda, M.A. Martin-Lara, G. Blázquez, N.M. Bachs, M. Calero, Copper biosorption in the presence of lead onto olive stone and pine bark in batch and continuous systems, Environ. Prog. Sustainable Energy, 33 (2013) 192–204.
[15] M.A. Shouman, N.A. Fathy, S.A. Khedr, A.A. Attia, Comparative biosorption studies of hexavalent chromium ion onto raw and modified palm branches, Adv. Phys. Chem., 2013 (2013) 9 p, doi.org/10.1155/2013/159712
[16] S.L. Goertzen, K.D. Thériault, A.M. Oickle, A.C. Tarasuk, H.A. Andreas, Standardization of the Boehm titration. Part I. $CO_2$ expulsion and endpoint determination, Carbon, 48 (2010) 1252–1261.
[17] N.M. Hilal, A.A. Emam, A.A. El-Bayaa, N.A. Badawy, A.E. Zidan, Adsorption of barium and iron ions from aqueous solutions by the activated carbon produced from mazot ash, Life Sci. J., 10 (2013) 75–83.
[18] S. Lagergren, About the theory of so-called adsorption of soluble substances, K. Sven. Vetenskapsakad. Handl., 24 (1898) 1–39.
[19] Y.S. Ho, G. McKay, The kinetics of sorption of divalent metal ions onto Sphagnum moss peat, Water Res., 34 (2000) 735–742.
[20] W.J. Weber, J.C. Morris, Kinetics of adsorption on carbon from solution, J. Sanitary Eng. Div., 89 (1963) 31–60.
[21] E.S. Dragan, D. Humelnicu, M.V. Dinu, R.I. Olariu, Kinetics, equilibrium modelling, and thermodynamics on removal of Cr(VI) ions from aqueous solution using novel composites with strong base anion exchanger microspheres embedded into chitosan/poly(vinyl amine) cryogels, Chem. Eng. J., 330 (2017) 675–691.
[22] K.Y. Foo, B.H. Hameed, Insights into the modeling of adsorption isotherm systems, Chem. Eng. J., 156 (2010) 2–10.
[23] S.K. Papageorgiou, F.K. Katsaros, E.P. Kouvelos, N.K. Kanellopoulos, Prediction of binary adsorption isotherms of $Cu^{2+}$, $Cd^{2+}$ and $Pb^{2+}$ on calcium alginate beads from single adsorption data, J. Hazard. Mater., 162 (2009) 1347–1354.
[24] V.C. Srivastava, I.D. Mall, I.M. Mishra, Equilibrium modelling of single and binary adsorption of cadmium and nickel onto bagasse fly ash, Chem. Eng. J., 117 (2006) 79–91.
[25] H.N. Tran, S.-J. You, A. Hosseini-Bandegharaei, H.-P. Chao, Mistakes and inconsistencies regarding adsorption of contaminants from aqueous solutions: a critical review, Water Res., 120 (2017) 88–116.
[26] H.K. Goering, P.J. Van Soest, Forage Fiber Analyses (Apparatus, Reagents, Procedures, and Some Applications), US Government Printing Office, Washington, D.C., 1970.
[27] M. Mahmood-ul-Hassan, V. Suthar, E. Rafique, R. Ahmad, M. Yasin, Kinetics of cadmium, chromium, and lead sorption onto chemically modified sugarcane bagasse and wheat straw, Environ. Monit. Assess., 187 (2015) 470.
[28] W.S. Trahanovsky, Oxidation in Organic Chemistry: Organic Chemistry, A Series of Monographs, Academic Press, New York, 1982.
[29] N.A. Medellin-Castillo, E. Padilla-Ortega, M.C. Regules-Martínez, R. Leyva-Ramos, R. Ocampo-Pérez, C. Carranza-Alvarez, Single and competitive adsorption of Cd(II) and Pb(II) ions from aqueous solutions onto industrial chili seeds (Capsicum annuum) waste, Sustainable Environ. Res., 27 (2017) 61–69.
[30] N. Feng, X. Guo, S. Liang, Adsorption study of copper (II) by chemically modified orange peel, J. Hazard. Mater., 164 (2009) 1286–1292.
[31] M. Kostić, M. Radović, J. Mitrović, M. Antonijević, D. Bojić, M. Petrović, A. Bojić, Using xanthated Lagenaria vulgaris shell biosorbent for removal of Pb(II) ions from wastewater, J. Iran. Chem. Soc., 11 (2014) 565–578.
[32] I. Anastopoulos, M. Panagiotou, C. Ehaliotis, P.A. Tarantilis, I. Massas, NaOH pretreatment of compost derived from olive tree pruning waste biomass greatly improves biosorbent characteristics for the removal of $Pb^{2+}$ and $Ni^{2+}$ from aqueous solutions, Chem. Ecol., 31 (2015) 724–740.
[33] C.G. Boeriu, D. Bravo, R.J.A. Gosselink, J.E.G. van Dam, Characterisation of structure-dependent functional properties of lignin with infrared spectroscopy, Ind. Crops Prod., 20 (2004) 205–218.
[34] V.K. Gupta, A. Rastogi, Biosorption of lead from aqueous solutions by green algae spirogyra species: kinetics and equilibrium studies, J. Hazard. Mater., 152 (2008) 407–414.
[35] H. Qiu, L.V. Lu, B.-C. Pan, Q.-J. Zhang, W.-M. Zhang, Q.-X. Zhang, Critical review in adsorption kinetic models, J. Zhejiang Univ. Sci. A, 10 (2009) 716–724.
[36] M. Sanchez-Polo, J. Rivera-Utrilla, Adsorbent-adsorbate interactions in the adsorption of Cd(II) and Hg(II) on

ozonized activated carbons, Environ. Sci. Technol., 36 (2002) 3850–3854.
[37] N. Ayawei, A.N. Ebelegi, D. Wankasi, Modelling and interpretation of adsorption isotherms, J. Chem., 2017 (2017) 11 p. doi.org/10.1155/2017/3039817
[38] W.M. Ibrahim, Biosorption of heavy metal ions from aqueous solution by red macroalgae, J. Hazard. Mater., 192 (2011) 1827–1835.
[39] E. Pehlivan, B.H. Yanik, G. Ahmetli, M. Pehlivan, Equilibrium isotherm studies for the uptake of cadmium and lead ions onto sugar beet pulp, Bioresour. Technol., 99 (2008) 3520–3527.
[40] S. Doyurum, A. Çelik, Pb(II) and Cd(II) removal from aqueous solutions by olive cake, J. Hazard. Mater., 138 (2006) 22–28.
[41] G. Limousin, J.-P. Gaudet, L. Charlet, S. Szenknect, V. Barthès, M. Krimissa, Sorption isotherms: a review on physical bases, modeling and measurement, Appl. Geochem., 22 (2007) 249–275.
[42] Q. Li, S. Wu, G. Liu, X. Liao, X. Deng, D. Sun, Y. Hu, Y. Huang, Simultaneous biosorption of cadmium(II) and lead(II) ions by pretreated biomass of Phanerochaete chrysosporium, Sep. Purif. Technol., 34 (2004) 135–142.